Acta Pharmaceutica Sinica B 2022;12(3):1406−1415

Chinese Pharmaceutical Association
Institute of Materia Medica, Chinese Academy of Medical Sciences

Acta Pharmaceutica Sinica B

www.elsevier.com/locate/apsb
www.sciencedirect.com

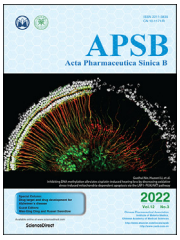

ORIGINAL ARTICLE

Discovery and development of brain-penetrant ^{18}F-labeled radioligands for neuroimaging of the sigma-2 receptors

Ying Zhang[a], Tao Wang[a], Xiaojun Zhang[b], Winnie Deuther-Conrad[c], Hualong Fu[a], Mengchao Cui[a], Jinming Zhang[b,*], Peter Brust[c,e], Yiyun Huang[d,*], Hongmei Jia[a,*]

[a]*Key Laboratory of Radiopharmaceuticals (Beijing Normal University), Ministry of Education, College of Chemistry, Beijing Normal University, Beijing 100875, China*
[b]*Nuclear Medicine Department, Chinese PLA General Hospital, Beijing 100853, China*
[c]*Helmholtz-Zentrum Dresden-Rossendorf, Institute of Radiopharmaceutical Cancer Research, Department of Neuroradiopharmaceuticals, Leipzig 04318, Germany*
[d]*PET Center, Department of Radiology and Biomedical Imaging, Yale University School of Medicine, New Haven, CT 06520-8048, USA*
[e]*The Lübeck Institute of Experimental Dermatology, University Medical Center Schleswig-Holstein, Lübeck 23538, Germany*

Received 28 May 2021; received in revised form 19 August 2021; accepted 20 August 2021

KEY WORDS

Indole-based derivatives;
σ_2 receptor;
Fluorine-18;
Positron emission tomography;
Neuroimaging

Abstract We have discovered and synthesized a series of indole-based derivatives as novel sigma-2 (σ_2) receptor ligands. Two ligands with high σ_2 receptor affinity and subtype selectivity were then radiolabeled with F-18 in good radiochemical yields and purities, and evaluated in rodents. In biodistribution studies in male ICR mice, radioligand [^{18}F]**9**, or 1-(4-(5,6-dimethoxyisoindolin-2-yl)butyl)-4-(2-[^{18}F]fluoroethoxy)-1*H*-indole, was found to display high brain uptake and high brain-to-blood ratio. Pretreatment of animals with the selective σ_2 receptor ligand CM398 led to significant reductions in both brain uptake (29%−54%) and brain-to-blood ratio (60%−88%) of the radioligand in a dose-dependent manner, indicating high and saturable specific binding of [^{18}F]**9** to σ_2 receptors in the brain. Further, *ex vivo* autoradiography in male ICR mice demonstrated regionally heterogeneous specific binding of [^{18}F]**9** in the brain that is consistent with the distribution pattern of σ_2 receptors. Dynamic positron emission tomography imaging confirmed regionally distinct distribution and high levels of specific binding for [^{18}F]**9** in

*Corresponding authors. Tel.: +86 10 58807843, fax: +86 10 58802750 (Hongmei Jia); Tel.: +1 203 7853193, fax: +1 203 7852994 (Yiyun Huang); Tel./fax: +86 10 68282330 (Jinming Zhang).
E-mail addresses: zhangjm301@163.com (Jinming Zhang), henry.huang@yale.edu (Yiyun Huang), hmjia@bnu.edu.cn (Hongmei Jia).
Peer review under responsibility of Chinese Pharmaceutical Association and Institute of Materia Medica, Chinese Academy of Medical Sciences.

https://doi.org/10.1016/j.apsb.2021.08.029

the rat brain, along with appropriate tissue kinetics. Taken together, results from our current study indicated the novel radioligand [^{18}F]**9** as the first highly specific and promising imaging agent for σ_2 receptors in the brain.

1. Introduction

Malfunctions in cholesterol homeostasis and lipid metabolism are involved in various human diseases[1−7]. Recently, the sigma-2 (σ_2) receptor has been identified as transmembrane protein 97 (TMEM97)[8], which is also named meningioma-associated protein (MAC30) and suggested to be a cholesterol-regulating gene[9]. Accordingly, much attention has been paid to the mechanism and role of the σ_2 receptor/TMEM97 in regulating cholesterol homeostasis and its implications in diseases[2,10,11]. The σ_2 receptor/TMEM97 was shown to have approximately 10-fold higher expression in proliferating than quiescent tumors[12−14], indicating the σ_2 receptor/TMEM97 as a biomarker for the proliferative status of solid tumors. TMEM97, progesterone receptor membrane component 1 (PGRMC1) and low-density lipoprotein receptor (LDLR) were reported to form a trimeric complex in HeLa cells. This complex accelerates the internalization of LDL in proliferating versus quiescent tumor cells[15], which is in good agreement with the up- and down-regulation of the σ_2 receptor/TMEM97 in 66P and 66Q cells[14]. Moreover, the TMEM97/PGRMC1/LDLR complex is a binding site for monomeric and oligomeric amyloid β-peptide (1−42) (Aβ_{1-42})[16]. Inhibition of one of these proteins results in the disruption of the TMEM97/PGRMC1/LDLR complex, leading to decreased uptake of Aβ_{1-42} in primary neurons[16]. Hence the σ_2 receptor/TMEM97 is also considered a therapeutic target for Alzheimer's disease (AD). For example, CT1812, a σ_2 receptor antagonist, is reported to prevent the binding of Aβ oligomers to neuronal receptors and thus holds potential as a novel drug for the treatment of AD[17−20]. The availability of a radioligand for neuroimaging of the σ_2 receptor/TMEM97 in the human brain will make it possible to investigate this target in AD progression, and to elucidate the treatment mechanism of CT1812 in clinical trials.

During the last decades, efforts in the development of σ_2 receptor radioligands have been largely directed toward *in vivo* imaging of tumors, where upregulation of σ_2 receptor is found[21−23]. Currently, *N*-(4-(6,7-dimethoxy-3,4-dihydroisoquinolin-2(1*H*)-yl) butyl)-2-(2-fluoroethyl)-5-methylbenzamide ([^{18}F]ISO-1) is the only σ_2 receptor radiotracer used in humans for tumor imaging[24−26]. However, it is not suitable to investigate σ_2 receptors in AD due to its low brain uptake[27]. With the aim to develop radioligands with appropriate affinity for the σ_2 receptor, high selectivity, high uptake, favorable kinetics and high specific binding in the brain, we chose compound **1** with nanomolar affinity and favorable selectivity for σ_2 receptor as the lead compound and introduced an methoxy or fluoroethoxy group at the different positions of the indole ring to enable the incorporation of ^{11}C or ^{18}F for PET imaging (Fig. 1)[28]. Previous structure−activity relationship studies showed that ligands with a four-carbon chain between the indole ring and the 6,7-dimethoxy-1,2,3,4-tetrahydroisoquinoline or 5,6-dimethoxyisoindoline moiety possessed high σ_2 receptor affinity and selectivity[29]. Two radioligands, [^{18}F]**8** and [^{18}F]**11**, were synthesized and evaluated in rodents, which showed [^{18}F]**11**, with a 6-[^{18}F]fluoroethoxy group at the indole ring and a 5,6-dimethoxyisoindoline moiety, displayed relatively good brain uptake but only moderate specific binding to the σ_2 receptors *in vivo*. In an effort to search for radioligands with optimized pharmacokinetic and *in vivo* binding properties, we further investigated the effects of the [^{18}F]fluoroethoxy group at different positions of the indole ring. Herein we report the synthesis of these indole-based derivatives and evaluation of two new ^{18}F-labeled radiotracers, [^{18}F]**9** and [^{18}F]**10**, for their potential to image σ_2 receptors in the brain.

2. Results

2.1. Chemical synthesis

The synthetic routes for target compounds **2**−**7** are illustrated in Scheme 1. Based on the method reported previously[28], *N*-alkylation of compounds **12**−**14** with 1,4-dibromobutane led to intermediates **15**−**17**. Reaction with 6,7-dimethoxy-1,2,3,4-tetrahydroisoquinoline or 5,6-dimethoxyisoindoline then provided target compounds **2**−**7**. Compounds **8**−**11** has been reported previously[29].

2.2. In vitro binding assays

Compounds **2**−**7** were assayed for their *in vitro* binding properties as previously reported[30,31]. The results are provided in Table 1. Introduction of methoxy group at the indole ring retained the nanomolar affinity for σ_2 receptors [K_i (σ_2) = 4.40−9.46 nmol/L] and moderate subtype selectivity [K_i (σ_1)/K_i (σ_2) = 7−102]. Compounds with 6,7-dimethoxy-1,2,3,4-tetrahydroisoquinoline displayed higher subtype selectivity towards σ_2 receptors than those with a 5,6-dimethoxyisoindoline moiety (compare **2**−**4** to **5**−**7**).

In general, compounds with a fluoroethoxy substituent (**8**−**11**) possessed higher affinity and subtype selectivity than those with a methoxy group (**2**−**7**). Therefore, compounds with the methoxy substituent were not pursued for further studies. Instead, we radiofluorinated the two compounds in the fluoroethoxy substituted series, *i.e.*, [^{18}F]**9** and [^{18}F]**10** with high affinity and selectivity for σ_2 receptors, to investigate the effects of the [^{18}F]fluoroethoxy position at the indole ring on *in vivo* properties and evaluate their potential as σ_2 receptor neuroimaging agents.

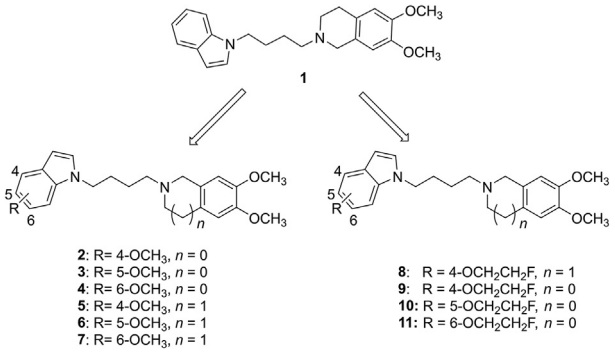

Figure 1 Design concept of indole-based derivatives as new σ_2 ligands.

2.3. *Radiochemistry*

Synthesis of the radiolabeling precursors and radiosynthesis of radioligands [^{18}F]**9** and [^{18}F]**10** are depicted in Scheme 2. Intermediates **20** and **21** were obtained by reaction of 4-(benzyloxy)-1*H*-indole (**18**) or 5-(benzyloxy)-1*H*-indole (**19**) with 1,4-dibromobutane under basic conditions. *N*-Alkylation of 5,6-dimethoxyisoindoline with **20** and **21** provided **22** and **23**, respectively. Debenzylation in the presence of H_2 and 10% Pd on activated carbon as catalyst provided compounds **24** and **25**. Further reaction with ethane-1,2-diyl bis(4-methylbenzenesulfonate) afforded compounds **26** and **27** as radiolabeling precursors.

Different from the synthetic methods previously described for [^{18}F]**8** and [^{18}F]**11**, we employed for the radiosynthesis of [^{18}F]**9** and [^{18}F]**10** an efficient one-step S_N2 reaction with [^{18}F]fluoride as reported in the literature[32], with retention times of 16.06 and 16.16 min on the chromatograms from semipreparative radio-high performance liquid chromatography (radio-HPLC, Supporting Information Fig. S1), radiochemical yields (RCYs) of 36%−50% (n = 10, decay-corrected) and 20%−29% (n = 5, decay-corrected), molar activity of 29−151 GBq/μmol (n = 10) and 55−72 GBq/μmol (n = 5), respectively, for [^{18}F]**9** and [^{18}F]**10**, and radiochemical purity (RCP) of >99%. The total synthesis time was about 60 min. The RCYs for [^{18}F]**9** and [^{18}F]**10** from the one-step radiosynthesis were considerably higher than those for [^{18}F]**8** (10%−15%) and [^{18}F]**11** (16%−21%) prepared from a two-step procedure reported previously[29].

Identity of the radioligand [^{18}F]**9** or [^{18}F]**10** was confirmed by co-injection with the corresponding reference compound **9** or **10** into an analytical HPLC system. The chromatograms are shown in Supporting Information Fig. S2, indicating co-elution of the labeled and unlabeled compounds. The retention times were 8.53 and 8.61 min for **9** and [^{18}F]**9**, and 8.19 and 8.31 min for **10** and [^{18}F]**10**, respectively, with the slight differences in retention times accounted for the distance between the UV and gamma detectors of the HPLC system.

Table 1 *In vitro* binding properties of the indole-based ligands[a].

Compd.	K_i (σ_1) (nmol/L)	K_i (σ_2) (nmol/L)	K_i (σ_1)/K_i (σ_2)
2	149 ± 67	6.30 ± 2.00[c]	24
3	190 ± 97	8.91 ± 1.40	21
4	70 ± 14	9.46 ± 1.20[c]	7
5	259 ± 23	7.73 ± 4.49[c]	33
6	450 ± 89	4.40 ± 1.43[c]	102
7	357 ± 94	8.68 ± 1.99	41
8[b]	1698 ± 548	2.40 ± 0.58	708
9[b]	371 ± 105	1.79 ± 0.86	207
10[b]	187 ± 1.41	3.27 ± 0.19	57
11[b]	376 ± 351	2.63 ± 0.48	143

[a]Values are the means ± standard deviation (SD) of at least two independent experiments, each done in triplicate.
[b]From Ref. 29.
[c]n = 2.

2.4. *In vitro and in vivo assessments*

2.4.1. *In vitro stability*

Radioligands [^{18}F]**9** and [^{18}F]**10** were incubated in saline at ambient temperature or in mouse serum at 37 °C for 2 h to determine their stability *in vitro*. The RCP remained at >99% as shown in Supporting Information Fig. S3, suggesting high stability of [^{18}F]**9** and [^{18}F]**10** *in vitro*.

2.4.2. *Lipophilicity*

Radioligands [^{18}F]**9** and [^{18}F]**10** were partitioned between 1-octanol and 0.05 mol/L potassium phosphate buffer (pH 7.4) to measure their log$D_{7.4}$, which were 2.43 ± 0.01 (n = 3) and 2.29 ± 0.01 (n = 3), respectively, for [^{18}F]**9** and [^{18}F]**10**, well within the optimal range for good blood–brain barrier (BBB) permeability[33].

2.4.3. *Biodistribution and blocking experiments in mice*

Biodistribution experiments were performed in male ICR mice. The results are presented in Tables 2 and 3. Initial uptake in the brain, at 2 min post-injection (p.i.), was observed to be higher for

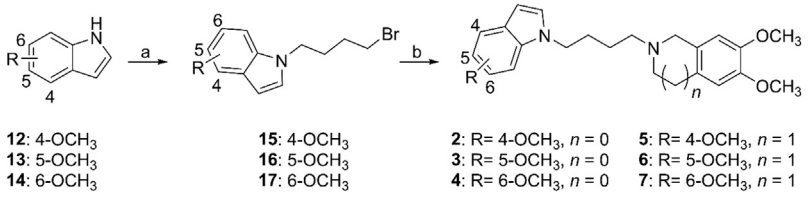

Scheme 1 Synthetic route for target compounds with a methoxy group at the indole ring. Reagents and conditions: (a) DMF, 1,4-dibromobutane, KOH, TBAF (1 mol/L in THF), r.t., 2 h, 52%−72%; (b) acetonitrile, triethylamine, K_2CO_3, 5,6-dimethoxyisoindoline/6,7-dimethoxy-1,2,3,4-tetrahydroisoquinoline, 90 °C, 5 h, 55%−77%.

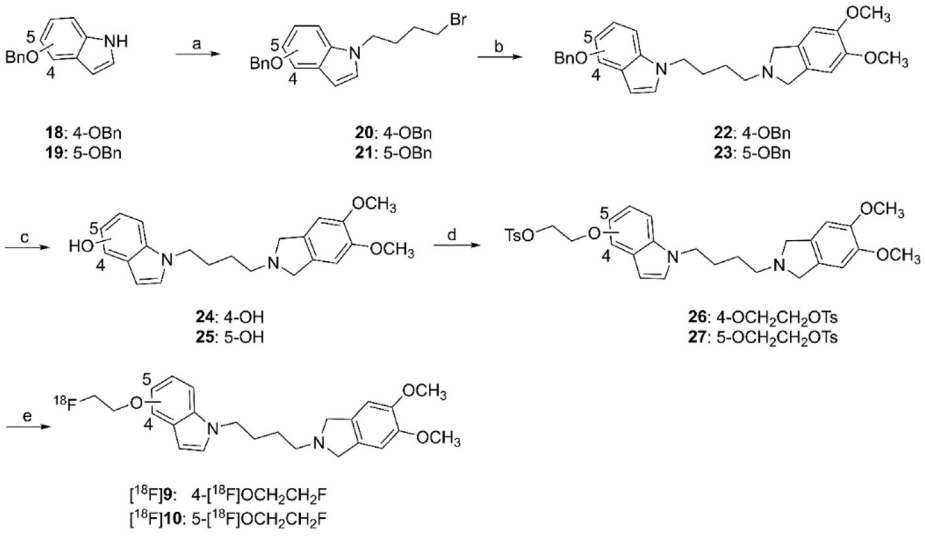

Scheme 2 Synthesis of precursors **26** and **27** and radiosynthesis of [^{18}F]**9** and [^{18}F]**10**. Reagents and conditions: (a) DMF, 1,4-dibromobutane, KOH, 0 °C−r.t., 2 h, 47%−64%; (b) 5,6-dimethoxyisoindoline, acetonitrile, K_2CO_3, triethylamine, 90 °C, 2.5 h, 51%−79%; (c) H_2, Pd/C, CH_3OH, 50 °C, 63%−74%; (d) ethane-1,2-diyl bis(4-methylbenzenesulfonate), acetonitrile, KOH, 90 °C, 20 min, for **26**, 59%; for **27**, 17%; (e) [^{18}F]F^-, Kryptofix 2.2.2, K_2CO_3, CH_3CN, 100 °C, 5 min.

[^{18}F]**9** (4.44 ± 0.59% ID/g) than [^{18}F]**10** (3.76 ± 0.28% ID/g). Ligand [^{18}F]**9** showed the highest uptake in the brain (5.04 ± 0.67% ID/g) at 30 min, indicating a slow clearance. On the other hand, [^{18}F]**10** showed relatively fast brain washout, with level of uptake at 120 min only 42% of that at 2 min. The blood level of [^{18}F]**9** was low with 0.48 ± 0.08% ID/g at 30 min and 0.42 ± 0.05% ID/g at 60 min p.i., which led to high brain-to-blood ratios of 10.6 at both time points. The highest brain-to-blood ratio (3.13) was seen at 15 min for [^{18}F]**10**.

To verify the binding specificity of [^{18}F]**9** and [^{18}F]**10** to σ_2 receptors *in vivo*, blocking experiments in male ICR mice were conducted by pre-administration (5 min prior to ∼280 kBq of radiotracer) of **9** (0.1 mL, 3 μmol/kg), **10** (0.1 mL, 3 μmol/kg), and various concentrations of CM398 (0.1 mL; 3, 5, 10 or 20 μmol/kg), a selective σ_2 receptor ligand[34]. The blocking effects on [^{18}F]**9** and [^{18}F]**10** at 30 min p.i. are summarized in Fig. 2. For [^{18}F]**9**, animals pre-treated with CM398 showed a dose-dependent reductions in brain uptake levels (29%−54%), and brain-to-blood ratios (60%−88%). Activity levels were also reduced in the heart (66%−77%), spleen (55%−65%), lungs (73%−82%) and kidneys (73%−76%). Similarly, self-blocking led to remarkable reductions of radioactivity concentrations in the above organs.

For [^{18}F]**10**, pretreatment with compound **10** or CM398 led to slightly reduced activity uptake in the brain (8%−18%). The brain-to-blood ratio also decreased (37%−47%). In addition, radioactivity levels were reduced in the liver (30%−42%), spleen (47%−54%), and kidneys (31%−33%). Overall the blocking effect was smaller for [^{18}F]**10** than [^{18}F]**9**, indicating lower levels of specific binding for [^{18}F]**10**.

2.4.4. *Effect of P-gp on radioligand uptake in the brain*

P-glycoprotein (P-gp), which is highly expressed on the BBB, can restrict the brain penetration of molecules[35]. Male ICR mice were treated with cyclosporine A, a P-gp inhibitor, at 60 min before radioligand administration to assess its effect on brain uptake of [^{18}F]**9** and [^{18}F]**10**. The results are presented in Fig. 3. A slight increase without significance in blood uptake was observed for [^{18}F]**9** and [^{18}F]**10** ($P > 0.05$). The initial brain uptake levels at 2 min p.i were significantly increased by 49% and 67% ($P < 0.05$) for [^{18}F]**9** and [^{18}F]**10**, respectively. Moreover, the brain-to-blood ratios were significantly increased by 35% and 50% for [^{18}F]**9** and [^{18}F]**10**, respectively, in the groups treated with cyclosporine A ($P < 0.05$), suggesting that [^{18}F]**9** and [^{18}F]**10** are moderate P-gp substrates.

2.4.5. *Ex vivo autoradiography in mice*

Given the more favorable binding property observed for [^{18}F]**9** in biodistribution studies, *ex vivo* autoradiography study was conducted to investigate its levels of uptake and specific binding in mouse brain regions. The results are presented in Figs. 4–7. Radioactivity was widely and heterogeneously distributed in the mouse brain. High levels of accumulation were observed in the cortex, cerebellum, olfactory bulb, midbrain and lateral ventricle, similar to the results reported in the literature[36]. Uptake level was moderate in the striatum, and low in the thalamus and hippocampus. The pattern of distribution in the brain for [^{18}F]**9** is clearly different from that we recently obtained with a σ_1 receptor radioligand[37].

When the mice were injected with CM398 (5 μmol/kg) or compound **9** (3 μmol/kg) at 5 min before radiotracer injection and sacrificed at 30 min p.i. for autoradiography, levels of radiotracer accumulation were dramatically reduced in all brain regions (Figs. 4–7), with significant differences ($P < 0.001$) found in the cortex, hippocampus, midbrain, cerebellum, striatum, thalamus and olfactory bulb. The blocking effect averaged across brain regions was similar to that seen for the whole brain in the biodistribution study, reaffirming the high level of specific binding for [^{18}F]**9** in the brain.

2.4.6. *Micro-PET/CT imaging in rats*

Encouraged by the favorable properties of [^{18}F]**9** in mice, imaging experiments in Sprague−Dawley (SD) rats were performed on a

Table 2 Biodistribution of [^{18}F]**9** in mice[a].

Organ	2 min	15 min	30 min	60 min	120 min
Blood	2.39 ± 0.36	0.70 ± 0.08	0.48 ± 0.08	0.42 ± 0.05	0.42 ± 0.03
Brain	4.44 ± 0.59	4.95 ± 0.36	5.04 ± 0.67	4.43 ± 0.39	3.41 ± 0.13
Heart	21.57 ± 1.58	11.23 ± 0.91	7.55 ± 1.30	3.49 ± 0.62	2.76 ± 0.41
Liver	3.24 ± 0.67	6.13 ± 0.94	8.69 ± 0.44	10.97 ± 0.95	11.9 ± 1.52
Spleen	5.01 ± 1.80	7.51 ± 1.17	9.93 ± 1.43	11.35 ± 2.85	10.51 ± 0.37
Lung	108.47 ± 20.11	36.37 ± 6.47	17.93 ± 2.42	9.95 ± 1.62	7.53 ± 1.07
Kidney	18.89 ± 2.48	18.40 ± 2.45	20.61 ± 1.80	17.40 ± 3.97	12.36 ± 0.81
Pancreas	8.74 ± 0.29	12.75 ± 2.12	18.93 ± 2.95	22.66 ± 3.36	24.21 ± 1.57
Small intestine[b]	6.21 ± 0.81	7.27 ± 0.88	10.80 ± 0.36	10.73 ± 1.27	10.88 ± 0.38
Stomach[b]	1.21 ± 0.14	1.52 ± 0.19	1.54 ± 0.20	1.39 ± 0.27	1.22 ± 0.13
Muscle	4.38 ± 0.99	3.74 ± 0.33	3.90 ± 0.23	3.01 ± 0.51	3.01 ± 0.27
Bone	2.59 ± 0.66	3.02 ± 0.45	4.50 ± 0.38	4.64 ± 1.57	5.57 ± 0.53
Brain/Blood	1.87 ± 0.13	7.21 ± 1.36	10.57 ± 1.86	10.56 ± 0.83	8.11 ± 0.37

[a]Data shown are percentage of injected dose per gram of tissue (% ID/g), means ± SD, $n = 5$.
[b]% ID/organ.

Table 3 Biodistribution of [^{18}F]**10** in mice[a].

Organ	2 min	15 min	30 min	60 min	120 min
Blood	2.77 ± 0.10	1.19 ± 0.09	1.19 ± 0.17	1.46 ± 0.12	1.89 ± 0.18
Brain	3.76 ± 0.28	3.70 ± 0.26	2.68 ± 0.27	1.69 ± 0.16	1.58 ± 0.16
Heart	15.47 ± 1.37	3.54 ± 0.13	2.36 ± 0.26	2.03 ± 0.21	2.31 ± 0.16
Liver	7.42 ± 1.66	14.65 ± 2.01	18.09 ± 1.16	18.32 ± 1.60	14.57 ± 2.33
Spleen	6.18 ± 1.09	11.32 ± 1.27	8.69 ± 0.95	6.13 ± 0.29	4.31 ± 0.50
Lung	61.17 ± 6.95	14.05 ± 3.06	7.10 ± 1.12	5.18 ± 0.83	3.41 ± 0.51
Kidney	19.00 ± 1.41	14.96 ± 1.49	8.75 ± 0.97	6.18 ± 1.02	3.94 ± 0.57
Pancreas	11.70 ± 2.14	23.72 ± 2.35	34.10 ± 3.60	39.66 ± 2.95	43.39 ± 6.87
Small intestine[b]	7.47 ± 0.93	12.37 ± 0.25	15.81 ± 1.40	18.14 ± 1.20	20.49 ± 1.33
Stomach[b]	1.62 ± 0.54	2.87 ± 0.32	2.83 ± 0.54	2.54 ± 0.43	3.54 ± 0.74
Muscle	5.60 ± 0.91	2.72 ± 0.96	2.48 ± 0.18	1.93 ± 0.17	1.86 ± 0.20
Bone	3.40 ± 1.14	4.40 ± 0.88	5.11 ± 0.68	5.19 ± 0.84	6.49 ± 1.23
Brain/Blood	1.36 ± 0.08	3.13 ± 0.35	2.29 ± 0.40	1.16 ± 0.16	0.85 ± 0.16

[a]Data shown are percentage of injected dose per gram of tissue (% ID/g), means ± SD, $n = 5$.
[b]% ID/organ.

micro-positron emission tomography (PET)/computed tomography (CT) scanner to further investigate the pharmacokinetic and binding characteristics of [^{18}F]**9** in the brain. After administration of [^{18}F]**9**, dynamic PET scan was acquired for 120 min. PET images are shown in Fig. 8. Presented in Fig. 9 are the whole brain and regional time−activity curves (TACs) from both the baseline and CM398 blocking scans. The highest levels of uptake were found in the cerebellum and cortex, followed by the hippocampus, midbrain, striatum and thalamus. Pretreatment with CM398 (10 μmol/kg) at 5 min prior to the injection of [^{18}F]**9** resulted in markedly decreased uptake in the above brain regions with faster washout. Radiotracer accumulation in the whole-brain was remarkably reduced (>60%) after 30 min. These findings confirmed regionally distinct distribution of [^{18}F]**9** in the rat brain, and its high levels of specific binding to σ_2 receptors.

2.4.7. In vivo metabolic stability

The brain and pancreas of ICR mice were dissected at 30 min after injection of [^{18}F]**9** (0.2 mL, 33.3 MBq), processed, and analyzed by HPLC to examine the presence (or absence) of radioactive metabolites in these tissues. Representative radio-HPLC chromatograms are presented in Supporting Information Fig. S4. In the brain samples, the parent compound [^{18}F]**9** accounted for ≥95% of the radioactivity signal, indicating negligible entry of radio-metabolites into the brain. In contrast, only about ~10% of the signal in pancreas was attributable to radiotracer [^{18}F]**9** ($n = 3$), with the rest from radio-metabolites.

3. Discussion

The σ_2 receptor has been considered as a putative therapeutic target for neurological diseases[19,20,38,39]. However, to date there has been no suitable radioligand for imaging this receptor subtype in the brain, as previous efforts in σ_2 radioligand development were primarily targeted for tumor imaging. Therefore, we set out to develop brain-penetrant radioligands with high σ_2 affinity and subtype selectivity for neuroimaging applications. Indole-based derivatives with the 6,7-dimethoxy-1,2,3,4-tetrahydroisoquinoline or 5,6-dimethoxyisoindoline pharmacophore as reported here and previously exhibited nanomolar affinity for σ_2 receptors. Replacement of the methoxy substituent in the indole ring with fluoroethoxy group appeared to increase both σ_2 affinity and subtype selectivity (**2**−**7** *vs.* **8**−**11**). As a result, we focused on radioligands with the [^{18}F]fluoroethoxyindole moiety for development and evaluation as potential σ_2 neuroimaging agents.

In our previous work, we synthesized and evaluated two radioligands [^{18}F]**8** and [^{18}F]**11**, and found that they indeed

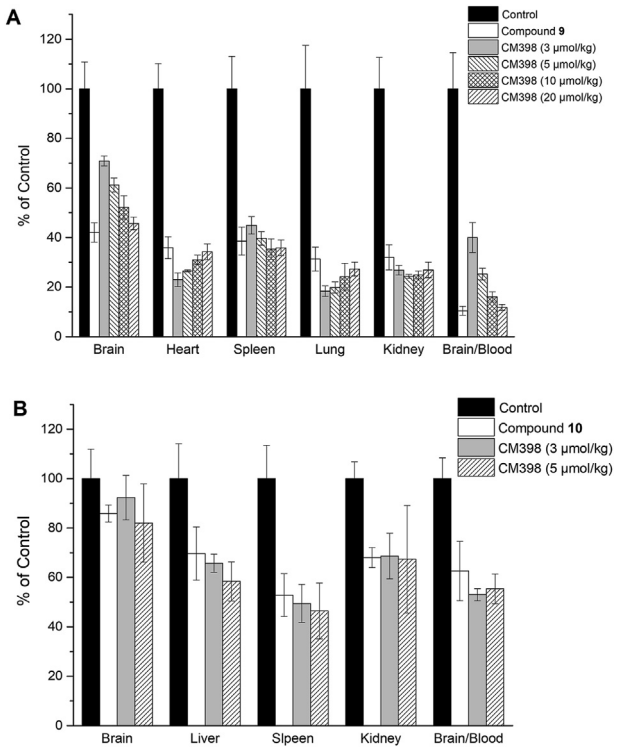

Figure 2 Effects of pre-administration with compound **9** (0.1 mL, 3 μmol/kg), compound **10** (0.1 mL, 3 μmol/kg), or ascending doses of CM398 (3, 5, 10 or 20 μmol/kg) on biodistribution of (A) [^{18}F]**9** and (B) [^{18}F]**10** at 30 min p.i. All values are means ± SD (n = 5−6 for each group). Student's t test (independent, two-tailed), $P < 0.001$ for [^{18}F]**9** and $P < 0.05$ for [^{18}F]**10** (except for CM398 effect in the brain).

entered the brain well[29]. Nonetheless, the level of specific binding was only moderate, and radioligand [^{18}F]**8**, with the 6,7-dimethoxy-1,2,3,4-tetrahydroisoquinoline pharmacophore, demonstrated less favorable *in vivo* kinetic and binding characteristics. In a continued effort to search for σ_2 radioligands with improved kinetic and imaging properties, we further synthesized radioligands [^{18}F]**9** and [^{18}F]**10** with the [^{18}F]fluoroethoxy group at the 4- and 5-position of the indole ring, respectively, and the less lipophilic 5,6-dimethoxyisoindoline pharmacophore.

As indicated by the results from biodistribution studies reported previously[29], compared to [^{18}F]**9**, radiotracer [^{18}F]**8**, with the 6,7-dimethoxy-1,2,3,4-tetrahydroisoquinoline pharmacophore exhibited lower initial brain uptake (3.29% ID/g at 2 min *vs.* 4.44% ID/g for [^{18}F]**9**) and lower brain-to-blood ratio (3.0 at 15 min *vs.* 7.2 for [^{18}F]**9**). Moreover, blocking with compound **11** led to only 24% reduction in brain uptake, suggesting low level of specific binding to σ_2 receptors in the brain. So we focused on ligands with the 5,6-dimethoxyisoindoline pharmacophore to further investigate the effects of [^{18}F]fluoroethoxy at the different positions of the indole ring on brain kinetics and specific binding.

Listed in Table 4 for comparison are the *in vitro* and *in vivo* characteristics of radioligands [^{18}F]**9**, [^{18}F]**10** and [^{18}F]**11**, with the [^{18}F]fluoroethoxy moiety at the 4-, 5-, or 6-position of the indole ring, respectively. Similar to [^{18}F]**11**, the two new radioligands [^{18}F]**9** and [^{18}F]**10** displayed the appropriate lipophilicity required for BBB permeability of neuroimaging agents, and good *in vitro* stability. Both *in vitro* binding affinity for σ_2 receptor and σ_2/σ_1 subtype selectivity followed the order of [^{18}F]**9** > [^{18}F]**11** > [^{18}F]**10**. Radioligands [^{18}F]**9** and [^{18}F]**11** displayed initial brain uptake at 2 min after injection (4.44% and 4.55% ID/g) higher than [^{18}F]**10** (3.76% ID/g), which are all much higher than that of the established σ_2 radioligand [^{18}F]ISO-1 (0.76% ID/g)[27]. Brain uptake at 30 min was similar for [^{18}F]**10** and [^{18}F]**11** (2.68% and 2.28% ID/g), but much higher for [^{18}F]**9** (5.04% ID/g), which is consistent with its highest σ_2 affinity [K_i (σ_2) = 1.79 ± 0.86 nmol/L] in this series. Radioligand [^{18}F]**9** also showed the highest brain-to-blood ratios, peaking at >10 between 30 and 60 min, compared with 3.0 and 5.0 for [^{18}F]**10** and [^{18}F]**11**, respectively, at 15 min after injection. Further, in self-blocking or CM-398 pretreatment experiments, [^{18}F]**9** displayed the most remarkable reduction of radioactivity levels in the brain, heart, spleen, lungs and kidneys, indicating that [^{18}F]**9** possessed the highest specific binding to σ_2 receptors *in vivo*. Most importantly, a dose-dependent blocking effect of CM398 on brain uptake and brain-to-blood ratios was observed, indicating highly specific and saturable binding of [^{18}F]**9** to σ_2 receptors in the brain. Finally, all three radiotracers showed relatively low levels of radioactivity uptake in the bone at 120 min, suggesting little defluorination of these radiotracers *in vivo*.

To elucidate the interaction between P-gp and [^{18}F]**9**, the effect of the P-gp inhibitor cyclosporine A on brain uptake of [^{18}F]**9** was tested in ICR mice. Pretreatment with cyclosporine A increased uptake of [^{18}F]**9** in both the brain and blood. The differences in brain uptake and brain-to-blood ratio between control and cyclosporine A-treated groups were significant ($P < 0.05$), indicating that [^{18}F]**9** is a moderate P-gp substrate. Results from the same set of experiments for [^{18}F]**10** and [^{18}F]**11** also indicated that they might be substrates for P-gp.

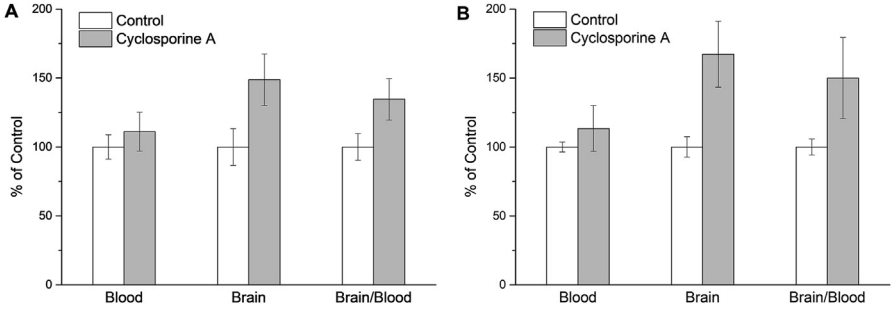

Figure 3 Effects of cyclosporine A on radioactivity levels of (A) [^{18}F]**9** and (B) [^{18}F]**10** in the mouse brain and blood (n = 5−8 per group). Student's t test (independent, two-tailed), for brain uptake and brain-to-blood ratio, $P < 0.05$ for both [^{18}F]**9** and [^{18}F]**10**. Data presented as means ± SD.

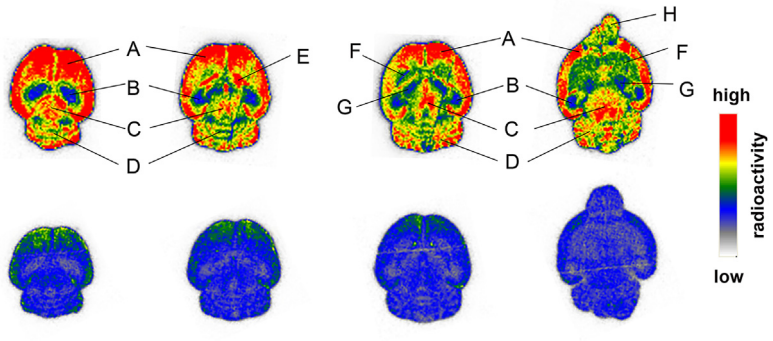

Figure 4 *Ex vivo* autoradiograms of [^{18}F]**9** in the mouse brain under baseline (upper row) and CM398 blocking (lower row) conditions: (A) Cortex; (B) Hippocampus; (C) Midbrain; (D) Cerebellum; (E) Lateral ventricle; (F) Striatum; (G) Thalamus; (H) Olfactory bulb.

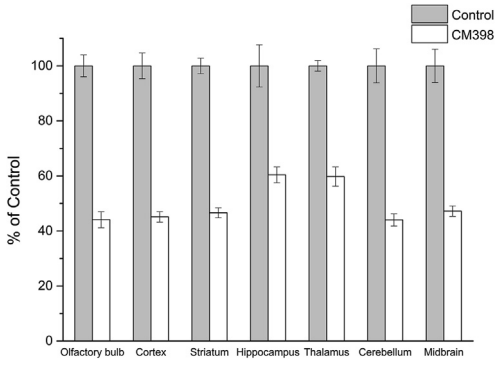

Figure 5 *Ex vivo* autoradiography results of [^{18}F]**9** in the mouse brain under baseline and CM398 blocking conditions. Student's *t* test (independent, two-tailed), $P < 0.001$ for all brain regions listed. Data presented as means ± SD, $n = 5$.

Since [^{18}F]**9** has the highest σ_2 specific binding in the brain in this series, *ex vivo* autoradiography experiments were conducted to further examine its distribution in brain regions. High levels of accumulation were found in the cortex, cerebellum and olfactory bulb, in line with results found with other σ_2 radioligands in the literature[36,40]. On the other hand, higher levels of accumulation in the midbrain and lateral ventricle were also observed, with lower levels in the hippocampus and thalamus, which are clearly different from the regional expression pattern of σ_1 receptors in the brain[32,37,41,42], and thus establishing that radioligand [^{18}F]**9** is evidently binding to the σ_2 receptors. These results verify that σ_1 and σ_2 receptors are distinctly and differently expressed in brain regions[43]. Pretreatment of animals with CM398 and compound **9** led to significant reductions in radiotracer uptake in different brain areas, further indicating the highly specific nature of [^{18}F]**9** binding to σ_2 receptors in the mouse brain and reaffirming the results from biodistribution studies.

Micro-PET/CT imaging was carried out in SD rats to further investigate the pharmacokinetic and binding properties of [^{18}F]**9** *in vivo*. After intravenous injection, [^{18}F]**9** entered the brain rapidly, then slowly washed out from different rat brain regions, consistent with the findings from biodistribution experiments in mice. Highest levels of uptake were observed in the cerebellum and cortex, followed by striatum, hippocampus, midbrain, and thalamus, in line with those found from *ex vivo* autoradiography study. Blocking with CM398 led to significant reductions in activity uptake to almost homogeneous levels in different brain regions, and much faster washout rates, demonstrating high specific binding of [^{18}F]**9** to σ_2 receptors in the rat brain.

Metabolism study in mice indicated that [^{18}F]**9** was the predominant radioactive species in the brain, with negligible amount of radio-metabolites, which is in good agreement with the high specific binding of [^{18}F]**9** in the mouse brain. However, only about 10% of the radioactivity was attributed to [^{18}F]**9** in the pancreas. As a result, there appeared to be little specific binding of [^{18}F]**9** in

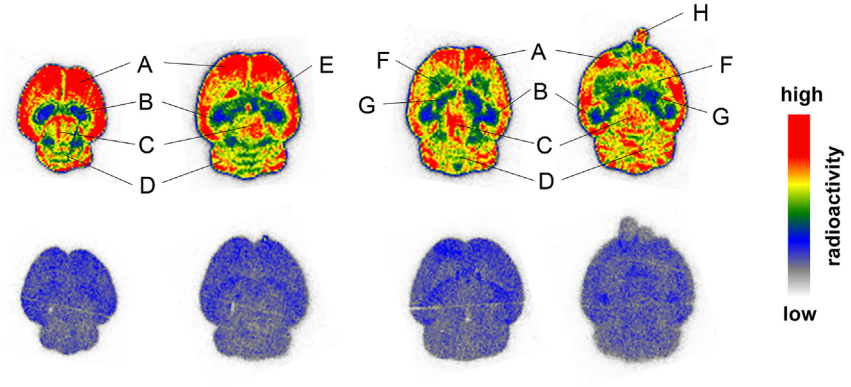

Figure 6 *Ex vivo* autoradiograms of [^{18}F]**9** in the mouse brain under baseline (upper row) and self-blocking (with compound **9** at 3 μmol/kg, lower row) conditions: (A) Cortex; (B) Hippocampus; (C) Midbrain; (D) Cerebellum; (E) Lateral ventricle; (F) Striatum; (G) Thalamus; (H) Olfactory bulb.

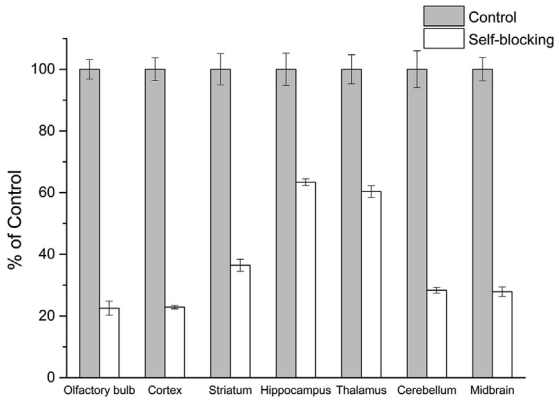

Figure 7 *Ex vivo* autoradiography results of [^{18}F]**9** in the mouse brain under baseline and self-blocking (with compound **9** at 3 μmol/kg) conditions. Student's *t* test (independent, two-tailed), $P < 0.001$ for all brain regions listed. Data presented as means ± SD, $n = 5$.

the mouse pancreas, although high activity level was observed in this organ.

4. Conclusions

Through structure−activity relationship studies, indole-based compounds with the 5,6-dimethoxyisoindoline pharmacophore, a four-carbon linker, and a fluoroethoxy substituent in the indole moiety were discovered to confer favorable properties as selective σ_2 receptor ligands. Three radioligands with the [^{18}F]fluoroethoxy group at different positions of the indole ring were prepared and found to readily enter the brain, thus fulfilling the first requirement as neuroimaging agents. Further *ex vivo* and *in vivo* evaluations identified radiotracer [^{18}F]**9**, with the highest *in vitro* binding affinity and subtype selectivity for σ_2 receptor, as the most favorable agent for neuroimaging. In rodents it exhibited the highest levels of brain uptake, brain-to-blood ratio, and specific binding among the σ_2 receptor radioligands reported to date. Combined with its appropriate kinetics in the brain, the novel radioligand [^{18}F]**9** from the current study is undoubtedly the most promising radioligand for neuroimaging of the σ_2 receptors, and thus warrants further evaluation in primates for its potential to image and quantitate cerebral σ_2 receptors in various brain diseases.

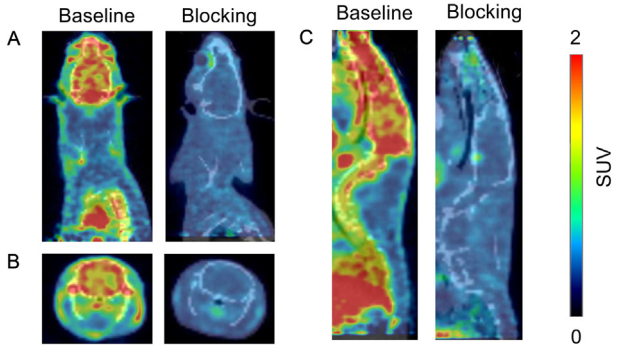

Figure 8 (A) Coronal, (B) axial and (C) sagittal rat brain micro-PET/CT fusion images summed from 30 to 45 min after injection of [^{18}F]**9** under baseline and CM398 (10 μmol/kg) blocking conditions.

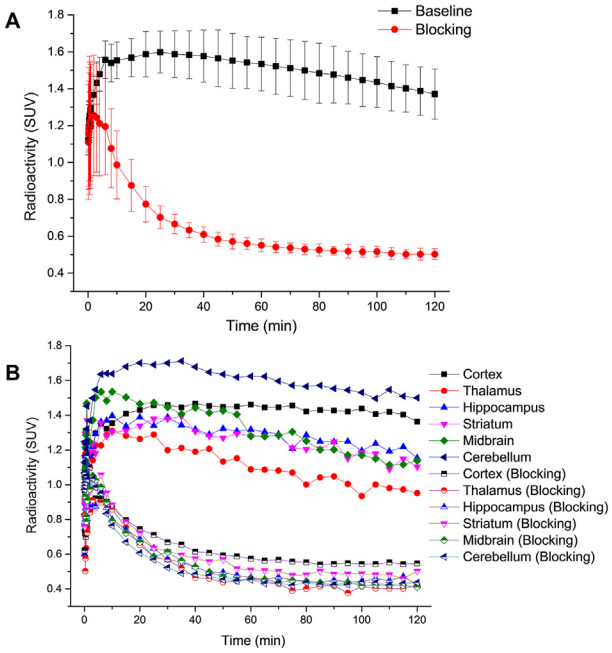

Figure 9 Time–activity curves of [^{18}F]**9** (A) in the whole-brain from baseline ($n = 3$) and CM398 (10 μmol/kg) blocking scans ($n = 3$), and (B) in selected brain regions from one baseline and one CM398 blocking scans in two separate rats. SUV = standardized uptake value.

5. Experimental

5.1. General information

The reagents and solvents, thin-layer chromatography (TLC) , ^{1}H NMR and ^{13}C NMR spectra, mass spectrometry (MS), high-resolution mass spectrometry (HRMS), HPLC, mice were obtained and handled in a manner similar to that reported in previous work[29,41]. Details are provided in the Supporting Information. Chemical synthesis and characterization data of intermediate and final compounds were provided in the Supporting Information. All the final compounds were characterized by ^{1}H NMR, ^{13}C NMR and HRMS. Chemical purities of ≥95% were indicated by NMR spectra and analysis with HPLC (see Supporting Information).

Normal male ICR mice (20 ± 2 g, 4−5 weeks) and male SD rats (200 ± 10 g, 6−7 weeks) were purchased from Vital River Experimental Animal Technical Co., Ltd. Experiments in animals were carried out in compliance with relevant regulations and institutional guidelines, and approved by the Institutional Animal Care and Use Committee of Beijing Normal University.

5.2. Radiochemistry

Synthesis of radiotracers[32], determination of log*D* value[42] and *in vitro* stability studies[42] followed the procedures reported previously. Detailed procedures are provided in the Supporting Information.

5.3. Biological evaluations

In vitro radioligand competition studies[30,31], *in vivo* biodistribution and blocking studies[42], effect of P-gp on brain uptake[29], *ex vivo* autoradiography[41], *in vivo* micro-PET/CT imaging

Table 4 Comparison of *in vitro* and *in vivo* characteristics for radioligands [^{18}F]**9**, [^{18}F]**10** and [^{18}F]**11**.

Property		Radioligand		
		[^{18}F]**9**	[^{18}F]**10**	[^{18}F]**11**[29]
K_i (σ_2) (nmol/L)		1.79 ± 0.86	3.27 ± 0.19	2.63 ± 0.48
K_i (σ_1)/K_i (σ_2)		207	57	143
Log$D_{7.4}$		2.43 ± 0.01	2.29 ± 0.01	2.17 ± 0.13
Brain uptake at 2 min (% ID/g)		4.44 ± 0.59	3.76 ± 0.25	4.55 ± 0.43
Brain uptake at 30 min (% ID/g)		5.04 ± 0.67	2.68 ± 0.25	2.28 ± 0.16
Brain/Blood ratio at 30 min		10.57	2.29	3.62
Self-blocking effect	Brain	58%	14%	21%
	Brain/Blood	90%	37%	68%
Blocking effect of CM398 (5 μmol/kg)	Brain	39%	18%	–
	Brain/Blood	75%	45%	–
P-gp substrate		Yes	Yes	Yes

–Not applicable.

in rats[32] and *in vivo* metabolism studies[29] followed the procedures reported previously. Detailed procedures are provided in the Supporting Information.

Acknowledgments

This work was supported by the National Natural Science Foundation of China (No. 21876013) and Beijing Natural Science Foundation (7212203, China).

Author contributions

All authors contributed to this manuscript and have approved the final article. Ying Zhang, Yiyun Huang and Hongmei Jia designed the study, participated in data analysis and interpretation and wrote the manuscript. Ying Zhang, Tao Wang and Xiaojun Zhang performed experiments. Winnie Deuther-Conrad and Peter Brust performed *in vitro* radioligand competition binding studies and participated in data analysis and interpretation. Hualong Fu, Mengchao Cui and Jinming Zhang designed and participated in experiments.

Conflicts of interest

The authors have no conflicts of interest to declare.

Appendix A. Supporting information

Supporting information to this article can be found online at https://doi.org/10.1016/j.apsb.2021.08.029.

References

1. Gabitova L, Gorin A, Astsaturov I. Molecular pathways: sterols and receptor signaling in cancer. *Clin Cancer Res* 2014;**20**:28–34.
2. Yang K, Zeng C, Wang C, Sun M, Yin D, Sun T. Sigma-2 receptor—a potential target for cancer/Alzheimer's disease treatment *via* its regulation of cholesterol homeostasis. *Molecules* 2020;**25**:5439.
3. Chang TY, Yamauchi Y, Hasan MT, Chang C. Cellular cholesterol homeostasis and Alzheimer's disease. *J Lipid Res* 2017;**58**:2239–54.
4. Matsushita Y, Nakagawa H, Koike K. Lipid metabolism in oncology: why it matters, how to research, and how to treat. *Cancers* 2021;**13**:474.
5. Mayengbam SS, Singh A, Pillai AD, Bhat MK. Influence of cholesterol on cancer progression and therapy. *Transl Oncol* 2021;**14**:101043.
6. Wellington CL. Cholesterol at the crossroads: Alzheimer's disease and lipid metabolism. *Clin Genet* 2004;**66**:1–16.
7. Lukiw WJ, Pappolla M, Pelaez RP, Bazan NG. Alzheimer's disease—a dysfunction in cholesterol and lipid metabolism. *Cell Mol Neurobiol* 2005;**25**:475–83.
8. Alon A, Schmidt HR, Wood MD, Sahn JJ, Martin SF, Kruse AC. Identification of the gene that codes for the σ_2 receptor. *Proc Natl Acad Sci U S A* 2017;**114**:7160–5.
9. Bartz F, Kern L, Erz D, Zhu M, Gilbert D, Meinhof T, et al. Identification of cholesterol-regulating genes by targeted RNAi screening. *Cell Metabol* 2009;**10**:63–75.
10. Shen H, Li J, Xie X, Yang H, Zhang M, Wang B, et al. BRD2 regulation of sigma-2 receptor upon cholesterol deprivation. *Life Sci Alliance* 2020;**4**:e201900540.
11. Zeng C, Riad A, Mach RH. The biological function of sigma-2 receptor/TMEM97 and its utility in PET imaging studies in cancer. *Cancers* 2020;**12**:1877.
12. Mach RH, Smith CR, Al-Nabulsi I, Whirrett BR, Childers SR, Wheeler KT. σ_2 receptors as potential biomarkers of proliferation in breast cancer. *Cancer Res* 1997;**57**:156–61.
13. Al-Nabulsi I, Mach RH, Wang LM, Wallen CA, Keng PC, Sten K, et al. Effect of ploidy, recruitment, environmental factors, and tamoxifen treatment on the expression of sigma-2 receptors in proliferating and quiescent tumour cells. *Br J Cancer* 1999;**81**:925–33.
14. Wheeler KT, Wang LM, Wallen CA, Childers SR, Cline JM, Keng PC, et al. Sigma-2 receptors as a biomaker of proliferaion in solid tumours. *Br J Cancer* 2000;**82**:1223–32.
15. Riad A, Zeng C, Weng CC, Winters H, Xu K, Makvandi M, et al. Sigma-2 receptor/TMEM97 and PGRMC-1 increase the rate of internalization of LDL by LDL receptor through the formation of a ternary complex. *Sci Rep* 2018;**8**:16845.
16. Riad A, Lengyel-Zhand Z, Zeng C, Weng CC, Lee VM, Trojanowski JQ, et al. The sigma-2 receptor/TMEM97, PGRMC1, and LDL receptor complex are responsible for the cellular uptake of Abeta42 and its protein aggregates. *Mol Neurobiol* 2020;**57**:3803–13.
17. Izzo NJ, Xu J, Zeng C, Kirk MJ, Mozzoni K, Silky C, et al. Alzheimer's therapeutics targeting amyloid beta 1-42 oligomers II: sigma-2/PGRMC1 receptors mediate Abeta 42 oligomer binding and synaptotoxicity. *PLoS One* 2014;**9**:e111899.
18. Izzo NJ, Staniszewski A, To L, Fa M, Teich AF, Saeed F, et al. Alzheimer's therapeutics targeting amyloid beta 1-42 oligomers I: Abeta 42 oligomer binding to specific neuronal receptors is displaced by drug candidates that improve cognitive deficits. *PLoS One* 2014;**9**:e111898.

19. Grundman M, Morgan R, Lickliter JD, Schneider LS, DeKosky S, Izzo NJ, et al. A phase 1 clinical trial of the sigma-2 receptor complex allosteric antagonist CT1812, a novel therapeutic candidate for Alzheimer's disease. *Alzheimers Dement* 2019;**5**:20−6.
20. Izzo NJ, Yuede CM, LaBarbera KM, Limegrover CS, Rehak C, Yurko R, et al. Preclinical and clinical biomarker studies of CT1812: a novel approach to Alzheimer's disease modification. *Alzheimers Dement* 2021;**17**:1365−82.
21. Huang YS, Lu HL, Zhang LJ, Wu Z. Sigma-2 receptor ligands and their perspectives in cancer diagnosis and therapy. *Med Res Rev* 2014;**34**:532−66.
22. Mach RH, Zeng C, Hawkins WG. The σ_2 receptor: a novel protein for the imaging and treatment of cancer. *J Med Chem* 2013;**56**:7137−60.
23. Zeng C, McDonald ES, Mach RH. Molecular probes for imaging the sigma-2 receptor: *in vitro* and *in vivo* imaging studies. *Handb Exp Pharmacol* 2017;**244**:309−30.
24. Dehdashti F, Laforest R, Gao F, Shoghi KI, Aft RL, Nussenbaum B, et al. Assessment of cellular proliferation in tumors by PET using ^{18}F-ISO-1. *J Nucl Med* 2013;**54**:350−7.
25. McDonald ES, Doot RK, Young AJ, Schubert EK, Tchou J, Pryma DA, et al. Breast cancer ^{18}F-ISO-1 uptake as a marker of proliferation status. *J Nucl Med* 2020;**61**:665−70.
26. Abramson Cancer Center of the University of Pennsylvania. Imaging of *in vivo* sigma-2 receptor expression with ^{18}F-ISO-1 positron emission tomography in metastatic breast cancer. *ClinicalTrials.gov Identifier* 2017. NCT03057743.
27. Tu Z, Xu J, Jones LA, Li S, Dumstorff C, Vangveravong S, et al. Fluorine-18-labeled benzamide analogues for imaging the σ_2 receptor status of solid tumors with positron emission tomography. *J Med Chem* 2007;**50**:3194−204.
28. Mesangeau C, Amata E, Alsharif W, Seminerio MJ, Robson MJ, Matsumoto RR, et al. Synthesis and pharmacological evaluation of indole-based sigma receptor ligands. *Eur J Med Chem* 2011;**46**:5154v61.
29. Wang L, Ye J, He Y, Deuther-Conrad W, Zhang J, Zhang X, et al. ^{18}F-Labeled indole-based analogs as highly selective radioligands for imaging sigma-2 receptors in the brain. *Bioorg Med Chem* 2017;**25**:3792−802.
30. Fan C, Jia H, Deuther-Conrad W, Brust P, Steinbach J, Liu B. Novel ^{99m}Tc labeled σ receptor ligand as a potential tumor imaging agent. *Sci China Ser B Chem* 2006;**49**:169−76.
31. Bautista-Aguilera OM, Budni J, Mina F, Medeiros EB, Deuther-Conrad W, Entrena JM, et al. Contilisant, a tetratarget small molecule for Alzheimer's disease therapy combining cholinesterase, monoamine oxidase inhibition, and H3R antagonism with S1R agonism profile. *J Med Chem* 2018;**61**:6937−43.
32. Li Y, Wang X, Zhang J, Deuther-Conrad W, Xie F, Zhang X, et al. Synthesis and evaluation of novel ^{18}F-labeled spirocyclic piperidine derivatives as σ_1 receptor ligands for positron emission tomography imaging. *J Med Chem* 2013;**56**:3478−91.
33. Patel S, Gibson R. *In vivo* site-directed radiotracers: a mini-review. *Nucl Med Biol* 2008;**35**:805−15.
34. Intagliata S, Sharma A, King TI, Mesangeau C, Seminerio M, Chin FT, et al. Discovery of a highly selective sigma-2 receptor ligand, 1-(4-(6,7-dimethoxy-3,4-dihydroisoquinolin-2(1*H*)-yl)butyl)-3-methyl-1*H*-benzo[*d*]imidazole-2(3*H*)-one (CM398), with drug-like properties and antinociceptive effects *in vivo*. *AAPS J* 2020;**22**:94.
35. Kreisl WC, Liow JS, Kimura N, Seneca N, Zoghbi SS, Morse CL, et al. P-glycoprotein function at the blood−brain barrier in humans can be quantified with the substrate radiotracer ^{11}C-*N*-desmethyl-loperamide. *J Nucl Med* 2010;**51**:559−66.
36. Abate C, Selivanova SV, Muller A, Kramer SD, Schibli R, Marottoli R, et al. Development of 3,4-dihydroisoquinolin-1(2*H*)-one derivatives for the Positron Emission Tomography (PET) imaging of σ_2 receptors. *Eur J Med Chem* 2013;**69**:920−30.
37. Tian J, He Y, Deuther-Conrad W, Fu H, Xie F, Zhang Y, et al. Synthesis and evaluation of new 1-oxa-8-azaspiro[4.5]decane derivatives as candidate radioligands for sigma-1 receptors. *Bioorg Med Chem* 2020;**28**:115560.
38. Sahn JJ, Mejia GL, Ray PR, Martin SF, Price TJ. Sigma 2 receptor/Tmem97 agonists produce long lasting antineuropathic pain effects in mice. *ACS Chem Neurosci* 2017;**8**:1801−11.
39. Lever JR, Miller DK, Green CL, Fergason-Cantrell EA, Watkinson LD, Carmack TL, et al. A selective sigma-2 receptor ligand antagonizes cocaine-induced hyperlocomotion in mice. *Synapse* 2014;**68**:73−84.
40. Søby KK, Mikkelsen JD, Meier E, Thomsen C. Lu 28-179 labels a σ_2-site in rat and human brain. *Neuropharmacology* 2002;**43**:95−100.
41. He Y, Xie F, Ye J, Deuther-Conrad W, Cui B, Wang L, et al. 1-(4-[^{18}F]Fluorobenzyl)-4-[(tetrahydrofuran-2-yl)methyl]piperazine: a novel suitable radioligand with low lipophilicity for imaging σ_1 receptors in the brain. *J Med Chem* 2017;**60**:4161−72.
42. Chen YY, Wang X, Zhang JM, Deuther-Conrad W, Zhang XJ, Huang Y, et al. Synthesis and evaluation of a ^{18}F-labeled spirocyclic piperidine derivative as promising σ_1 receptor imaging agent. *Bioorg Med Chem* 2014;**22**:5270−8.
43. Leitner ML, Hohmann AG, Patrick SL, Walker JM. Regional variation in the ratio of σ_1 to σ_2 binding in rat brain. *Eur J Pharmacol* 1994;**259**:65−9.